Nanostructured Single-Ion-Conducting Hybrid Electrolytes Based on Salty Nanoparticles and Block Copolymers

Irune Villaluenga,[†,‡,||] Sebnem Inceoglu,[‡] Xi Jiang,[§] Xi Chelsea Chen,[§,||] Mahati Chintapalli,[§,⊥] Dunyang Rita Wang,[§,⊥] Didier Devaux,[†,‡,||] and Nitash P. Balsara*[,†,‡,§,||]

[†]Energy Storage and Distributed Resources Division, [‡]Joint Center for Energy Storage Research (JCESR), and [§]Materials Sciences Division, Lawrence Berkeley National Laboratory, Berkeley, California 94720, United States

[||]Department of Chemical and Biomolecular Engineering and [⊥]Department of Material Science and Engineering, University of California, Berkeley, Berkeley, California 94720, United States

Ⓢ *Supporting Information*

ABSTRACT: We report on the synthesis and characterization of a series of microphase-separated, single-ion-conducting block copolymer electrolytes. Salty nanoparticles comprising silsesquioxane cores with covalently bound polystyrenesulfonyllithium (trifluoromethyl-sulfonyl)imide (PSLiTFSI) chains were synthesized by nitroxide-mediated polymerization. Hybrid electrolytes were obtained by mixing the salty nanoparticles into a microphase-separated polystyrene-*b*-poly(ethylene oxide) (SEO) block copolymer. Miscibility of PSLiTFSI and poly(ethylene oxide) (PEO) results in localization of the nanoparticles in the PEO-rich microphase. The morphology of hybrid electrolytes was determined by scanning transmission electron microscopy. We explore the relationship between the morphology and ionic conductivity of the hybrid. The transference number of the electrolyte with the highest ionic conductivity was measured by dc polarization to confirm the single-ion-conducting character of the electrolyte. Discharge curves obtained from lithium metal–hybrid electrolyte–FePO₄ batteries are compared to the data obtained from the batteries with a conventional block copolymer electrolyte.
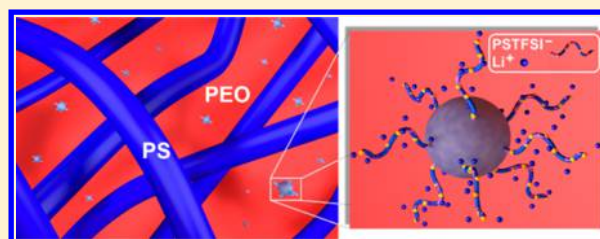
INTRODUCTION

Solid electrolytes in which the anions are immobile are of considerable interest in lithium batteries.[1] In these electrolytes, lithium ion transport occurs in the absence of concentration gradients, avoiding cell polarization and enhancing the power capability of the battery. Electrolytes with high modulus are essential for enabling high specific energy batteries with lithium metal anodes. One approach for obtaining high modulus electrolytes is through the use of microphase-separated block copolymers comprising a structural block to provide mechanical rigidity and a soft conducting block to provide avenues for ion transport.[2−4] A typical example of a such system is polystyrene-*b*-poly(ethylene oxide) (SEO) mixed with lithium trifluoro-methanesulfonylimide (LiTFSI). In these systems nanoscale polystyrene and poly(ethylene oxide)/LiTFSI domains are obtained by molecular self-assembly.

In an early study, Ryu et al. synthesized block copolymers with tethered anions and showed the importance of placing the anions in the non-conducting block.[5] At high temperatures (e.g., 70 °C), they obtained conductivities as high as 10^{-5} S/cm. It is, however, not clear if these highly conducting samples were microphase separated or not. In a subsequent publication, Bouchet et al. synthesized a triblock copolymer with a poly(ethylene oxide) block and two polystyrene end blocks with pendant trifluoromethanesulfonylimide anions (TFSI⁻) covalently bound to the styrene monomers and lithium counterions (Li⁺).[6] The bound nature of the TFSI⁻ anions

results in the lithium transference number close to unity. It was assumed in ref 6 that the copolymer was microphase separated. However, in subsequent studies it was shown that a significant ionic conductivity was only obtained in the disordered state wherein the ion-containing block and the PEO block were intimately mixed.[7,8] It is evident that designing microphase-separated single-ion-conducting block copolymer electrolytes is challenging. In this paper, we address this challenge by adding functionalized silsesquioxane nanoparticles to microphase-separated SEO block copolymer. Polystyrenesulfonyllithium (trifluoromethylsulfonyl)imide chains were covalently attached to the nanoparticles. The miscibility of these chains and PEO is well established.[7,8] The salty nanoparticles are thus expected to lie in the PEO-rich microdomains. We explore the relationship between morphology and conductivity as a function of nanoparticle concentration (or, equivalently, salt concentration) and temperature. Potentiostatic experiments are used to estimate lithium transference numbers. We compare charge–discharge curves of lithium metal–polymer electrolyte–FePO₄ batteries with our nanoparticle-containing SEO electrolyte and batteries with molecularly dissolved LiTFSI in SEO. We also show that the electrochemical stability window of nanoparticle-

containing SEO electrolytes is similar to that of SEO electrolytes with molecularly dissolved LiTFSI.

The phase behavior of nanoparticle/block copolymer mixtures has been studied extensively, e.g., refs 9−12. The importance of the particle size and surface modification was recognized in these studies. In particular, it was noted that interparticle aggregation can be avoided by ensuring that the particle diameter is significantly smaller than the size of the targeted domains. We used the results described in refs 9−12 to design our nanoparticle/block copolymer electrolytes.

■ EXPERIMENTAL SECTION

Single-Ion-Conducting Hybrid Block Copolymer Electrolytes Preparation. Salty nanoparticles (POSS-PSLiTFSI) were synthesized by nitroxide-mediated radical polymerization. First, acrylo-POSS particles were reacted with BlocBuilder MA to get POSS-based macroalkoxyamine. Then, the SKTFSI monomer was polymerized using the POSS-based macroalkoxyamine as the initiator in dimethylformamide at 115 °C, followed by the exchange of the cations K^+ to Li^+ by dialysis using a solution of lithium chloride to yield POSS−PSLiTFSI salty nanoparticles. The reaction yield was 77%, and the degree of polymerization was determined using inductively coupled plasma optical emission spectrometry (ICP-OES). POSS-PSLiTFSI nanoparticles contain 17.3 mg of lithium per particle (that is equivalent to 56 units of SLiTFSI per particle). The average number of monomers per chain is 7 (assuming that the chains emanate from all eight corners of a POSS nanoparticle); i.e., each particle has 56 lithium counterions. In addition, liquid ^1H NMR and ^{29}Si NMR (D_2O, Bruker AV600) were performed to confirm the chemical structure of the particles. Transmission electron microscopy (TEM) was performed to determine the size of the single-ion nanoparticles (POSS-PSLiTFSI). For this measurement, 1 wt % of the SEO/POSS-PSLiTFSI_0.085 sample was dissolved in DMF solutions at 90 °C for 16 h. 5 μL of the solution was then dropped onto a lacey carbon-coated copper grid, which was then suspended in a vial with a small amount of DMF to solvent anneal at room temperature for 45 min. The sample was then dried at 90 °C for 16 h. TEM experiments were performed on the Tecnai 12 in the Electron Microscope Lab in University of California at Berkeley, using 200 keV acceleration voltage.

Hybrid block copolymer electrolytes were prepared by the addition of different amounts of salty nanoparticles (POSS-PSLiTFSI) ($r =$ [Li]/[EO] = 0.02, 0.05, 0.085, and 0.10) to the SEO block copolymer in DMF. The solutions in DMF were cast and dried at 90 °C to obtain membranes with thicknesses between 100 and 200 μm. To ensure complete solvent removal, the hybrid electrolytes were subsequently dried overnight under vacuum at 90 °C in the glovebox antechamber. The characteristics of these electrolytes—the molar ratio of lithium atoms to ethylene oxide (EO) moieties, r, the weight fraction of the added POSS−PSLiTFSI nanoparticles, $w_{POSS−PSLiTFSI}$, and volume fraction of the conducting phase, ϕ_c—are summarized in Table 1.

The volume fraction of the conducting phase, ϕ_c, was calculated by eq 1:

$$\phi_c = \frac{v_{EO} + \frac{M_{POSS−PSLiTFSI}}{\rho_{POSS−PSLiTFSI} \cdot 56}}{v_{EO} + \frac{M_{POSS−PSLiTFSI}}{\rho_{POSS−PSLiTFSI} \cdot 56} + \frac{M_{PS}M_{EO}}{M_S M_{PEO}} v_S} \quad (1)$$

Table 1. Characteristics of Single-Ion-Conducting Hybrid Block Copolymer Electrolytes

name	$r =$ [Li]/[EO]	$w_{POSS−PSLiTFSI}$	ϕ_c
SEO/POSS-PSLiTFSI_0	N/A	N/A	0.49
SEO/POSS-PSLiTFSI_0.02	0.02	0.085	0.53
SEO/POSS-PSLiTFSI_0.05	0.05	0.189	0.58
SEO/POSS-PSLiTFSI_0.085	0.085	0.284	0.63
SEO/POSS-PSLiTFSI_0.10	0.10	0.318	0.64

where $\rho_{POSS−PSLiTFSI}$ is the density of POSS-PSLiTFSI nanoparticles (1.1 g/cm^3); v_{EO} and v_S are the molar volumes of EO monomer units (41.6 cm^3/mol) and styrene monomer units (107.4 cm^3/mol), respectively. $M_{POSS-PSLiTFSI}$, M_{PS}, M_{PEO}, M_S, and M_{EO} are the molar masses of POSS-PSLiTFSI nanoparticles (22.4 kg/mol), polystyrene (70 kg/mol), poly(ethylene oxide) (74 kg/mol), styrene (104.1 g/mol), and ethylene oxide (44.0 g/mol), respectively. We assume that the POSS−PSLiTFSI nanoparticles are located in the conducting block, i.e., in PEO microphase.

Battery Assembly and Testing. Inside the glovebox, a solution of hybrid electrolyte with $r = 0.085$ in NMP was stirred at 90 °C with LiFePO$_4$ and carbon black. The electrode formulation was 70 wt % LiFePO$_4$, 25 wt % SEO/POSS-PSLiTFSI_0.085, and 5 wt % carbon black. The resulting slurry was thoroughly mixed using a homogenizer inside an argon-filled glovebox. The slurry was then cast on aluminum foil using a doctor blade. The LiFePO$_4$ electrode was first dried overnight at 60 °C, followed by further drying at 90 °C in the glovebox antechamber under vacuum overnight. A disk of 1.1 cm diameter disk was punched from the LiFePO$_4$ electrode and pressed at 90 °C and 29 000 psi several times to reduce electrode porosity that resulted from the casting process. The electrode was hand-pressed at 90 °C onto the electrolyte, which was placed at the central hole (0.32 cm diameter) of an insulating spacer of 1.90 cm diameter. Then, a 1.27 cm diameter lithium disk was gently pressed onto the other side of the electrolyte. Aluminum and nickel tabs were taped on the LiFePO$_4$ and lithium electrodes, respectively, and the assembly was vacuum sealed in a pouch bag.

After assembly inside the glovebox, the batteries were transferred into an oven connected to a Maccor cycler where they were heated at 90 °C overnight prior to any cycling. The battery cycling rate is reported in term of C/n where n is the number of hours used to either charge or discharge the battery. Five conditioning charge−discharge cycles were performed at an approximate rate of $C/20$, using the estimated mass of LiFePO$_4$. Batteries were then charged at the target C rate using a constant current, I_c, until the potential reached 3.8 V. This was followed by a constant voltage step at 3.8 V. After a 1 h rest period, a discharge current, I_d (corresponding to the target C rate), was applied until the potential reached 2.5 V. After another 1 h rest period, another discharge step at $C/20$ was executed until the potential reached 2.5 V in an attempt to ensure complete discharge. We are mainly interested in discharge capacities obtained during the first step. At the end of each set of experiments on a given cell, it was charged and discharged at $C/20$ to ensure that there was no permanent change in cell capacity during the cycling at high C rates. Conventional batteries based on SEO/LiTFSI with $r = 0.085$ electrolytes were assembled and cycled at 90 °C under the conditions described by Devaux et al.[13] The characteristics of both batteries are summarized in Tables 2 and 3.

Table 2. Characteristics of the Hybrid Batteries Based on SEO/POSS-PSLiTFSI_0.085 Electrolyte

parameters	cathode	electrolyte (SEO/POSS-PSLiTFSI_0.085)	Li anode
thickness (μm)	23	30	150
diameter (cm)	1.11	0.32	1.27
composition (wt %, LiFePO$_4$:electrolyte:carbon)	70:25:5	N/A	N/A
electrode weight loading (mg/cm^2)	3.82	N/A	N/A

■ RESULTS AND DISCUSSION

POSS-PSLiTFSI nanoparticles are used as the source of lithium ions in our block copolymer electrolytes (Figure 1). In Figure 1a, we show a schematic of salty nanoparticles with the functional groups. Also shown in Figure 1a the results of NMR characterization of solutions of the salty nanoparticles in D_2O.

Table 3. Characteristics of the Conventional Batteries Based on SEO/LiTFSI with r = 0.085 Electrolyte

parameters	cathode	electrolyte (SEO/ LiTFSI_0.085)	Li anode
thickness (μm)	12	20	150
diameter (cm)	1.11	1.43	1.27
composition (wt %, LiFePO₄:electrolyte:carbon)	70:25:5	N/A	N/A
electrode weight loading (mg/cm²)	1.96	N/A	N/A
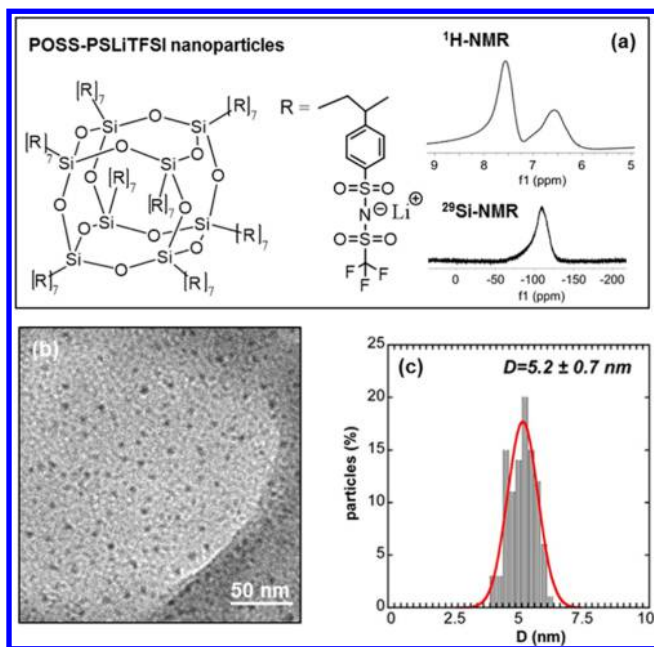
Figure 1. (a) Chemical structure of the salty nanoparticles (POSS-PSLiTFSI); ^{1}H NMR and ^{29}Si NMR spectra. (b) TEM image. (c) Size distribution of the POSS-PSLiTFSI nanoparticles.

^{1}H NMR shows characteristic peaks of the protons in styrene at 6.6 and 7.6 ppm. ^{29}Si NMR shows a single peak characteristic of silicon atoms in POSS at −110 ppm. A typical TEM image of the salty nanoparticles in the dry state is shown in Figure 1b.

Using such images, we determined the distribution of particle diameters (Figure 1c). The particles have narrow size distribution with an average diameter of 5.2 ± 0.7 nm.

The salty nanoparticles (POSS-PSLiTFSI) were mixed with the SEO block copolymer, resulting in hybrid electrolytes (SEO/POSS-PSLiTFSI_r) with different r values (r = [Li]/[EO] = 0.02, 0.05, 0.085, and 0.10).

The dependence of the ionic conductivity, σ, of the hybrid electrolytes with different nanoparticle loadings on temperature is shown in Figure 2a. The drop in conductivity at temperatures below 60 °C is due to PEO crystallization (see Supporting Information, Table S1). Differential scanning calorimetry (DSC) measurements indicate that the crystallinity of the hybrid electrolytes decreases with increasing salt concentrations (see Figure S1 and Table S1). The crystallinity of SEO/POSS-PSLiTFSI_0.02 is 56 % while that of SEO/POSS-PSLiTF-SI_0.10 is 20 %. However, T_m of all the hybrid electrolytes is independent of r values (between 61 and 63 °C). The POSS-PSLiTFSI nanoparticles impact the degree of crystallinity but not the temperature at which the PEO melts. We focus on ion transport at temperatures above the melting temperature (60−90 °C). In Figure 2b, we plot the σ versus r at 60 and 90 °C. Note the salt concentration, r, is fixed by nanoparticle loading. Regardless of temperature, σ is maximum with r = 0.085 (28.4 wt % of POSS-PSLiTFSI particles). This trend is similar to that found in PEO homopolymer/salt mixtures: the maximum occurs at r = 0.11 for 5 kg/mol PEO[14] and at r = 0.06 for 3.9−4.5 kg/mol PEO.[15] The T_g of homopolymer/salt sytems and SEO/salt systems increases with increasing salt concentration.[14] In contrast, the glass transition temperature of the PEO-rich domains (T_g(PEO)) in our hybrid electrolytes, measured by DSC, decreases from r = 0.085 and 0.10 (see Table S1). The decrease in conductivity when r is increasing from 0.085 to 0.10 in our hybrid electrolyte cannot be attributed to an increase in T_g, as is the case for conventional PEO/LiTFSI electrolytes.

Dry single-ion conductors exhibit conductivities that are significantly lower than mixtures of polymer and salts because the lithium ions have to hop between fixed anion sites. In the well-studied case of single-ion-conducting PSLiTFSI-PEO-PSLiTFSI and PEO-PSLiTFSI, measured conductivity values
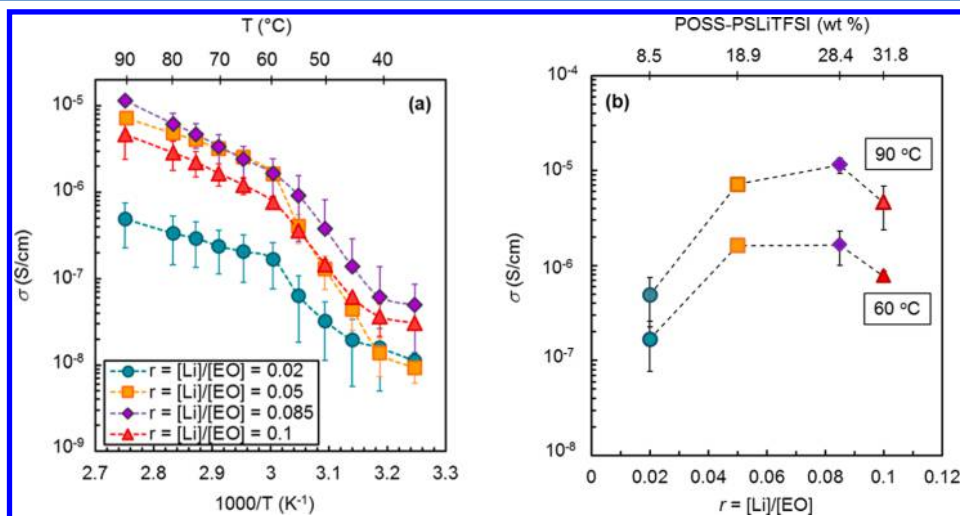
Figure 2. (a) Ionic conductivity, σ, of hybrid electrolytes (SEO/POSS-PSLiTFSI_r) versus the temperature. (b) Ionic conductivity, σ, versus salt concentration, r, at 60 and 90 °C. Nanoparticle weight percent is given on the top x-axis.

range from 3.3×10^{-5} to 1.6×10^{-4} S/cm.[6,8] The highest ionic conductivity in our SEO/POSS-PSLiTFSI ($r = 0.085$) is 1.1×10^{-5} S/cm, which is a factor of 3−15 lower than that of the pure block copolymers. This is due to the fact that, in addition to hops between fixed anions sites, the lithium ions must also hop from one nanoparticle to the next without access to counterions. It is important to note, however, that PEO-PSLiTFSI and PSLiTFSI-PEO-PSLiTFSI are disordered liquids in the conducting state while our SEO/POSS-PSLiTFSI ($r = 0.085$) is a rigid solid.

Figure 3 shows dark-field STEM images of all hybrid electrolytes ($r = 0.02$, 0.05, 0.085, and 0.10). The dark phase corresponds to the phase with lower electron density, i.e., PS-rich domains in the SEO block copolymer. It is evident that the morphology changes with the addition of salty nanoparticles. The hybrid electrolyte at low nanoparticle concentration ($r = 0.02$) exhibits a lamellar morphology. The hybrid electrolyte at high nanoparticle concentration ($r = 0.10$) exhibits a cylindrical morphology with wormlike PS-rich cylinders in a PEO-rich matrix. The morphology at $r = 0.085$ is similar to $r = 0.10$ except for the fact that the cylinders are highly disorganized. The STEM images at $r = 0.05$ contain regions of disorganized cylinders (along the diagonal in Figure 3b) coexisting with lamellae. It is not clear if the observed transition from lamellae to cylinders is due to differences in segregation strength or differences in volume fractions of microphases. The nanoparticles are not visible in Figure 3. This suggests that the nanoparticles are not clustered in the electrolytes.
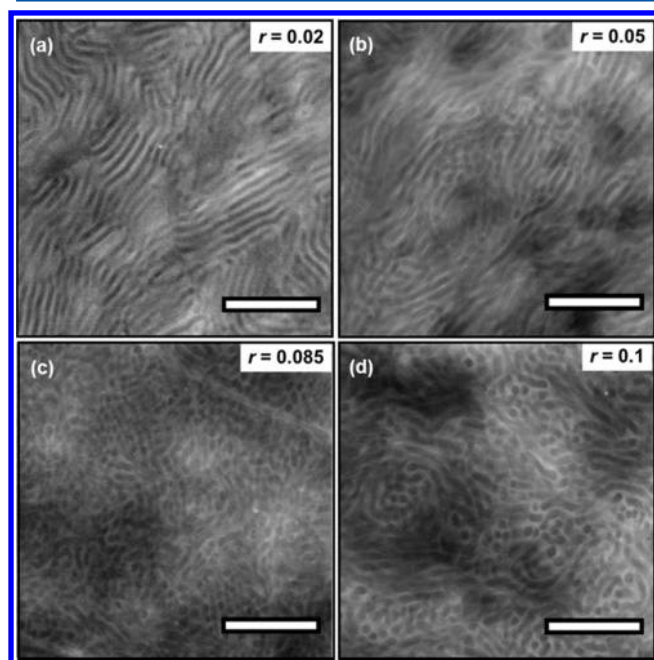
The location of the POSS-PSLiTFSI nanoparticles was determined by high resolution dark field STEM/EDS experiments (Figure 4). Elemental maps of carbon (C), silicon (Si), fluorine (F), and sulfur (S) were obtained for the optimum electrolyte ($r = 0.085$). Figure 4a shows the STEM image of the region of interest. It is evident that the dark PS-rich cylinders in Figure 4a have a high concentration of carbon (Figure 4b) while the bright PEO-rich matrix in Figure 4a has high concentrations of Si, S, and F (Figures 4c, 4d, and 4e). Figure 4f shows a composite map of all of the elements of interest. The POSS-PSLiTFSI particles are located in the PEO-rich matrix. This is due to the miscibility of the PSLiTFSI and PEO.[7,8]

SAXS profiles of the hybrid electrolytes at 90 °C are shown in Figure 5. All profiles contain a primary peak at $q = q^*$, indicating the presence of the periodic structures. The neat SEO only exhibits one peak, consistent with TEM images of the lamellar phase in ref 10. The hybrid electrolyte at low nanoparticle concentration ($r = 0.02$) exhibits a second-order scattering peak ($2q^*$), consistent with a lamellar morphology as seen in STEM (Figure 3a). The hybrid electrolyte at high nanoparticle concentration ($r = 0.10$) is consistent with a cylindrical morphology comprising cylinders with a radius, R, of 28 nm. We obtain this by assuming that the peak in the SAXS

Figure 3. HAADF-STEM images of hybrid electrolytes with (a) $r = 0.02$, (b) 0.05, (c) 0.085, and (d) 0.10. The scale bar for all images is 500 nm. The dark phase is PS-rich while the bright phase is PEO-rich.
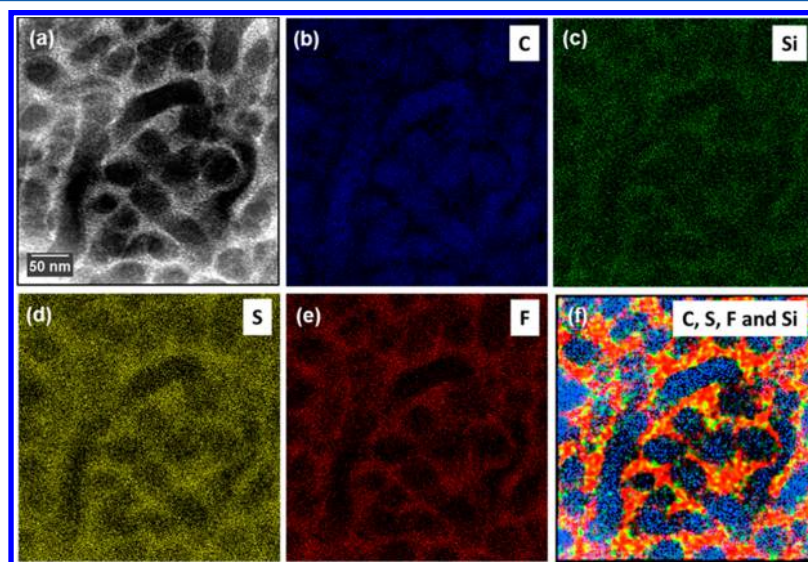

Figure 4. (a) STEM image of hybrid electrolyte with $r = 0.085$ and elemental maps of (b) carbon (C), (c) silicon (Si), (d) sulfur (S), and (e) fluorine (F). (f) Composite map of all of the elements (C = blue, S = yellow, F = red, and Si = green).
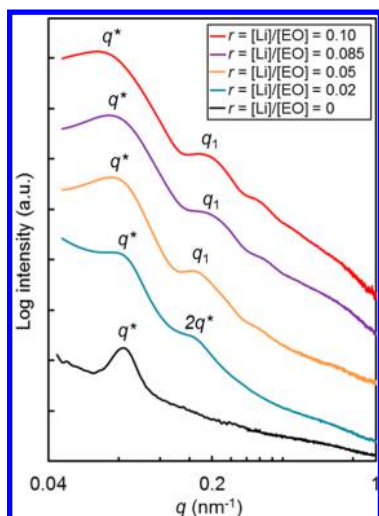
Figure 5. SAXS intensity versus the magnitude of the scattering vector, q, of hybrid block copolymer electrolytes (SEO/POSS-PSLiTFSI_r) with different r values at 90 °C.

profile of the $r = 0.10$ sample at $q_1 = 0.187$ nm^{-1} arises due to the first peak in the form factor of cylinders ($R = 5.3/q_1$). This is consistent with the cylindrical morphology seen in STEM (Figure 3d). The SAXS profiles obtain with $r = 0.05$ and $r = 0.085$ are also qualitatively consistent with the morphologies obtained by STEM (Figures 3b and 3c). The domain spacing (given by $d = 2\pi/q^*$), d_{SAXS}, increases as the salty nanoparticle concentration increases; $d_{SAXS} = 76.7$ nm with $r = 0.02$ and $d_{SAXS} = 94.8$ nm with $r = 0.10$.

In recent studies it was established that the conductivity of block copolymer electrolytes depends crucially on grain size.[14,16] In particular, it was found that reducing grain size increases conductivity. We thus propose that the reason for our observation that our hybrid electrolyte with $r = 0.085$ has a higher conductivity than $r = 0.10$ in spite of the fact that it contains a lower concentration of salty nanoparticles is due to differences in grain size. Some support for this claim is obtained by quantitative analysis of STEM images obtained from these two samples. We use the correlation length (ξ) as a metric to estimate the grain size. In Figures 6a and 6b, we show STEM images obtained from the $r = 0.085$ and $r = 0.10$ samples. The binary processed images of the samples are shown in Figures 6c and 6d. False color maps showing individual grains within which coherent order prevails are shown in Figures 6e and 6f. The correlation lengths obtained from this analysis are 24 ± 1.0 and 28.0 ± 1.3 nm for $r = 0.085$ and $r = 0.10$. This procedure (see Experimental Section for details) was repeated on three additional STEM images obtained from these samples (see Figure S2a,b). The values of ξ for the hybrid electrolyte with $r = 0.085$ range from 22.5 ± 0.8 to 31.7 ± 0.3 nm, with an average of 26.3 ± 4.0 nm. The values of ξ for the hybrid electrolyte with $r = 0.10$ range from 27.6 ± 0.5 to 53.5 ± 0.1 nm, with an average of 35.0 ± 12.0 nm. It is difficult to make definitive statements about the effect of salty nanoparticle concentration on grain size, given the wide range of ξ values obtained from each electrolyte. It appears that obtaining a reliable estimate of ξ will require analysis of a large number of STEM images. On the basis of the limited data we have thus far, we tentatively conclude that the grains in the $r = 0.085$ electrolyte are smaller than those in $r = 0.10$ electrolyte. (SAXS profiles could not be used to estimate the grain size because the peaks (Figure 5) are very broad and likely to be affected by factors other than grain size such as non-uniformity in domain spacing, contribution from nanoparticles, etc.)

Transference number measurements based on the Bruce–Vincent approach[17] (t^+_{BV}) were made on our hybrid electrolyte with $r = 0.085$, using a symmetric lithium–polymer–lithium cell. We measured the time-dependent current $I(t)$ obtained in response to a small dc potential. Ohm's law applies when a dc potential difference is applied across simple conductors with only one mobile charged species. On the other hand, in conventional electrolytes comprising two mobile charge carriers, concentration polarization leads to large deviations from Ohm's law. We define I_Ω to be the expected current if Ohm's law was obeyed. The sample resistance was measured by ac impedance before and after the application of dc potentials,
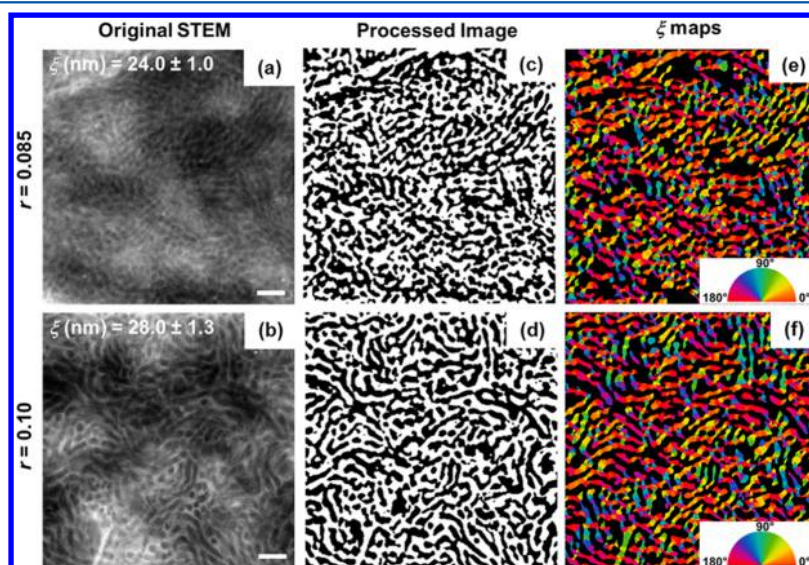

Figure 6. Original STEM images, (a, b) processed images (c, d), and correlation length maps (ξ maps, e, f) for hybrid electrolytes with $r = 0.085$ and $r = 0.10$ patterns. Correlation length maps are shown in false color to display the local orientation of each domain as used in the calculation of the correlation functions. The scale bar for all images is 200 nm.

and the results are shown in the inset of Figure 7. The sample resistance, R_{total}, is nearly independent of time. I_Ω is equal to
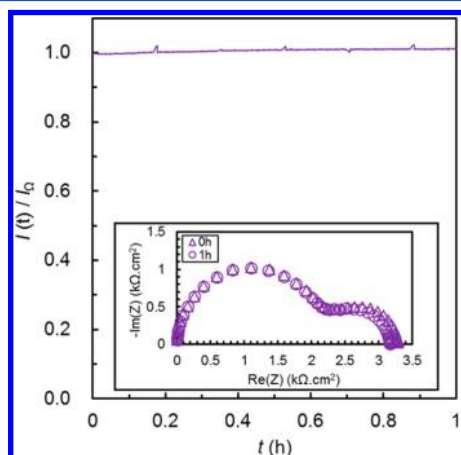

Figure 7. Normalized current density, $I(t)/I_\Omega$, as a function of time, t, for the hybrid electrolyte with $r = 0.085$ during an 80 mV polarization experiment in a symmetric lithium−hybrid−lithium cell at 90 °C. The inset shows the ac impedance of the cell before ($\triangle$) and after ($\bigcirc$) polarization.

$\Delta V/R_{total}$. (We used R_{total} measured before polarization to calculate I_Ω.) In Figure 7 we show $I(t)/I_\Omega$ versus time. $I(t)/I_\Omega$ is approximately 1 and independent of time. It is evident that our hybrid electrolyte obeys Ohm's law. The data in Figure 7 allow the evaluation of I_Ω, I^∞, R_{int}^0, and R_{int}^∞ and thus the calculation of t^+_{BV} (see Supporting Information, transference number measurements). We estimate that the lithium transference number, t^+_{BV}, is 0.98. This shows that most of the current in the hybrid electrolyte with $r = 0.085$ is carried by Li$^+$. In contrast, only a small fraction of the current in conventional PEO/salt electrolytes is carried by Li$^+$ ($t^+_{BV} \sim 0.1-0.3$).[18−20] To a good approximation, our hybrid electrolyte is a single-ion conductor. It is evident that our mixture of SEO and salty nanoparticles is microphase separated and that it is a single-ion conductor.

Cyclic voltammetry experiments were used to evaluate the electrochemical stability window of our hybrid electrolyte with $r = 0.085$ using a stainless steel−polymer−lithium cell. The dependence of current, I, on applied potential, E, is shown in the inset of Figure 8. The same experiment was repeated with a conventional block copolymer electrolyte (a mixture of SEO and LiTFSI with $r = 0.085$). The data obtained from this sample are also shown in the inset of Figure 8. The bulk resistance, R_{bulk}, of both samples was measured by ac impedance (1285.3 Ω cm^2 for the hybrid electrolyte and 32.5 Ω cm^2 for the conventional electrolyte). In Figure 8, we plot I/R_{bulk} versus E. It is evident that the electrochemical stability window of the hybrid electrolyte is similar to that of conventional block copolymer electrolyte (about 4 V vs Li$^+$/Li^0).

In order to investigate the viability of our single-ion-conducting hybrid electrolytes in devices, we built batteries with a lithium−metal negative electrode (anode), SEO/POSS-PSLiTFSI_0.085 electrolyte, and a composite positive electrode with LiFePO$_4$, carbon, and SEO/POSS-PSLiTFSI_0.085 (cathode). The potential window was between 2.5 and 3.8 V vs Li$^+$/Li^0 for battery cycling operation. Cycling tests were conducted at 90 °C with different rates, and we focus on the dependence of potential, E, on capacity, Q_d, during discharge
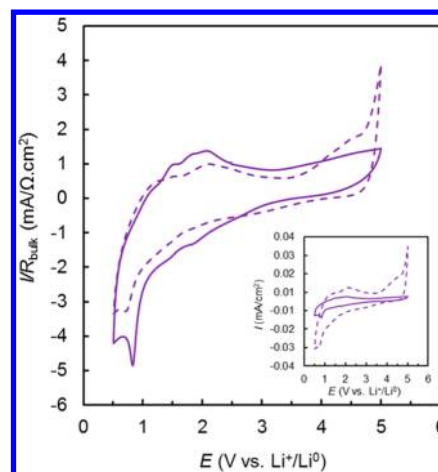

Figure 8. Normalized cyclic voltammograms of (—) the single-ion-conducting hybrid electrolyte with $r = 0.085$ and (- - -) a conventional SEO/LiTFSI block copolymer electrolyte with $r = 0.085$ obtained at 1 mV/s at 90 °C. The inset shows same data without normalization.

process. We compare our results with data obtained from very similar batteries with conventional block copolymer electrolyte (SEO/LiTFSI with $r = 0.085$) reported in ref 13 wherein both Li$^+$ and TFSI$^-$ are mobile. Details concerning the architecture of the two types of batteries are given in the Experimental Section. One expects better performance in the cell with SEO because the ionic conductivity of SEO/LiTFSI (5.6×10^{-4} S/cm) is a factor of 50 higher than that of SEO/POSS-PSLiTFSI_0.085 (1.1×10^{-5} S/cm) and because the thickness of the cathode in the SEO cell is lower. The data obtained from the conventional electrolyte cell are shown using dashed curves in Figure 9 while the data obtained from the single-ion-conducting hybrid electrolyte cell are shown using solid curves. The rate of discharge is characterized by C/n, where n is the number of hours used to fully discharge the cell. At low current densities corresponding to discharge rates $C/20$ and $C/15$, the two batteries exhibit similar behavior (Figure 9a). The discharge capacity of the single-ion-conducting battery is 163 mAh/g at $C/20$ and 158 mAh/g at $C/15$ (Figure 9a). At the same low current densities, the conventional battery presents similar discharge capacities (156 mAh/g at $C/20$ and 155 mAh/g at $C/15$). For higher discharge rates ($C/6$, $C/4$, and $C/2$), the accessible capacity decreases in both batteries (Figure 9b). This decrease is smaller for the conventional battery (149 mAh/g at $C/6$, 143 mAh/g $C/4$, and 133 mAh/g at $C/2$) than for the single-ion-conducting battery (131 mAh/g at $C/6$, 107 mAh/g $C/4$, and 67 mAh/g at $C/2$). At a given value of Q_d the potential obtained in SEO/POSS-PSLiTFSI_0.085 battery is between 0.05 and 0.2 lower than that obtained in SEO/LiTFSI_0.085 battery (Figure 9b). This is undoubtedly related to differences in the ionic conductivity. There is a qualitative difference between the discharge curves obtained from the two different kind of batteries (Figure 9). While all of the curves exhibit a "knee" near the end of discharge, the knee is much shaper in the single-ion-conducting battery. We attribute the differences between data obtained from SEO/POSS-PSLiTFSI_0.085 and SEO/LiTFSI_0.085 to the single-ion-conducting character of our hybrid electrolyte. While discharge profiles obtained from the batteries containing a conventional electrolyte with dissolved salt molecules are common in the literature,[21−25] relatively few studies have reported on the behavior on batteries with single-ion-conducting polymer
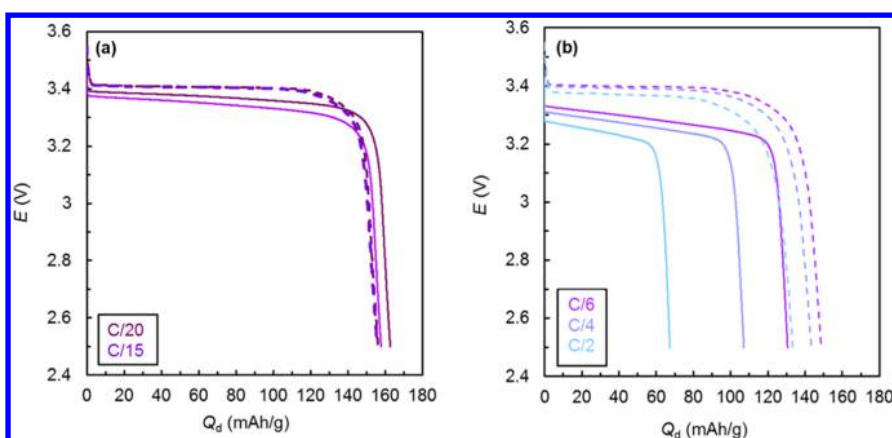
Figure 9. (a) Potential, E, as a function of the specific discharge capacity, Q_d, of (—) the single-ion-conducting hybrid battery (SEO/POSS-PSLiTFSI_0.085 as electrolyte) and (- - -) the conventional battery (SEO/LiTFSI with $r = 0.085$ as electrolyte) at different C rates: (a) C/20 and C/15 and (b) C/6, C/4, and C/2 at 90 °C.

electrolytes.[6,26] Our discharge curves are similar to those reported in ref 6 where a single-phase PEO-based single-ion conductor was used. Detailed modeling[27] is required to understand the reason for the differences in discharge curves presented in Figure 9. Such modeling is outside the scope of the present paper. While much work remains to be done, it is clear that the microphase-separated single-ion-conducting hybrid electrolytes developed here are viable for lithium metal batteries.

CONCLUSIONS

Novel salty nanoparticles comprising silsesquioxane cores with covalently bound polystyrenesulfonyllithium (trifluoromethyl-sulfonyl)imide (PSLiTFSI) chains were synthesized by nitroxide-mediated polymerization. The average number of monomers per chain is 7; i.e., each particle has 56 lithium counterions. Nanostructured single-ion-conducting hybrid electrolytes were obtained by mixing the salty nanoparticles into a microphase-separated SEO block copolymer. Miscibility of PSLiTFSI and PEO results in localization of the nanoparticles in the PEO-rich microphase. The effect of salty nanoparticle loading on morphology and conductivity was studied. A lamellar phase was obtained at low nanoparticle loading while a cylindrical phase with PS-rich cylinders was obtained at high nanoparticle loading. The ionic conductivity was optimized at an intermediate nanoparticle loading ($r = 0.085$) due to the effect of nanoparticles on morphology. The transference number of the optimum electrolyte, measured by the Bruce–Vincent approach, was close to unity. The electrochemical stability window of the single-ion-conducting hybrid electrolyte is similar to that of conventional SEO/LiTFSI electrolytes. The discharge curves of lithium metal–hybrid electrolyte–FePO$_4$ batteries are qualitatively different from those obtained with conventional electrolytes. We attribute this to the single-ion-conducting character of our hybrid electrolyte.

ASSOCIATED CONTENT

Ⓢ Supporting Information

The Supporting Information is available free of charge on the ACS Publications website at DOI: 10.1021/acs.macro-mol.6b02522.

Details on materials used, ac impedance characterization, transference number measurements, electrochemical window characterization, DSC profiles and thermodynamic data for the different hybrid electrolytes (SEO/POSS-PSLiTFSI_r), and morphology characterization details (and additional data of original STEM images, processed images, and correlation length maps (ξ maps) for hybrid electrolytes with (a) $r = 0.085$ and (b) $r = 0.10$ patterns) (PDF)

AUTHOR INFORMATION

Corresponding Author

*E-mail nbalsara@berkeley.edu, Ph (510) 642-8937 (N.P.B.).

ORCID

Irune Villaluenga: 0000-0002-1299-2479
Nitash P. Balsara: 0000-0002-0106-5565

Notes

The authors declare no competing financial interest.

■ REFERENCES

(1) Doyle, M.; Fuller, T. F.; Newman, J. The importance of the lithium ion transference number in lithium/polymer cells. *Electrochim. Acta* **1994**, *39*, 2073–2081.

(2) Giles, J. R. M.; Gray, F. M.; MacCallum, J. R.; Vincent, C. A. Synthesis and characterization of ABA block copolymer-based polymer electrolytes. *Polymer* **1987**, *28*, 1977–1981.

(3) Khan, I. M.; Fish, D.; Delaviz, Y.; Smid, J. ABA triblock comb copolymers with oligo(oxyethylene) side chains as matrix for ion transport. *Makromol. Chem.* **1989**, *190*, 1069–1078.

(4) Singh, M.; Odusanya, O.; Wilmes, G. M.; Eitouni, H. B.; Gomez, E. D.; Patel, A. J.; Chen, V. L.; Park, M. J.; Fragouli, P.; Iatrou, H.; Hadjichristidis, N.; Cookson, D.; Balsara, N. P. Effect of Molecular Weight on the Mechanical and Electrical Properties of Block Copolymer Electrolytes. *Macromolecules* **2007**, *40*, 4578–4585.

(5) Ryu, S.-W.; Trapa, P. E.; Olugebefola, S. C.; Gonzalez-Leon, J. A.; Sadoway, D. R.; Mayes, A. M. Effect of Counter Ion Placement on Conductivity in Single-Ion Conducting Block Copolymer Electrolytes. *J. Electrochem. Soc.* **2005**, *152*, A158–A163.

(6) Bouchet, R.; Maria, S.; Meziane, R.; Aboulaich, A.; Lienafa, L.; Bonnet, J.-P.; Phan, T. N. T.; Bertin, D.; Gigmes, D.; Devaux, D.; Denoyel, R.; Armand, M. Single-ion BAB triblock copolymers as highly efficient electrolytes for lithium-metal batteries. *Nat. Mater.* **2013**, *12*, 452–457.

(7) Inceoglu, S.; Rojas, A. A.; Devaux, D.; Chen, X. C.; Stone, G. M.; Balsara, N. P. Morphology–Conductivity Relationship of Single-Ion-Conducting Block Copolymer Electrolytes for Lithium Batteries. *ACS Macro Lett.* **2014**, *3*, 510–514.

(8) Rojas, A. A.; Inceoglu, S.; Mackay, N. G.; Thelen, J. L.; Devaux, D.; Stone, G. M.; Balsara, N. P. Effect of Lithium-Ion Concentration on Morphology and Ion Transport in Single-Ion-Conducting Block Copolymer Electrolytes. *Macromolecules* **2015**, *48*, 6589–6595.

(9) Garcia, B. C.; Kamperman, M.; Ulrich, R.; Jain, A.; Gruner, S. M.; Wiesner, U. Morphology Diagram of a Diblock Copolymer–Aluminosilicate Nanoparticle System. *Chem. Mater.* **2009**, *21*, 5397–5405.

(10) Villaluenga, I.; Chen, X. C.; Devaux, D.; Hallinan, D. T.; Balsara, N. P. Nanoparticle-Driven Assembly of Highly Conducting Hybrid Block Copolymer Electrolytes. *Macromolecules* **2015**, *48*, 358–364.

(11) Warren, S. C.; DiSalvo, F. J.; Wiesner, U. Nanoparticle-tuned assembly and disassembly of mesostructured silica hybrids. *Nat. Mater.* **2007**, *6*, 156–161.

(12) Kim, B. J.; Fredrickson, G. H.; Hawker, C. J.; Kramer, E. J. Nanoparticle Surfactants as a Route to Bicontinuous Block Copolymer Morphologies. *Langmuir* **2007**, *23*, 7804–7809.

(13) Devaux, D.; Harry, K. J.; Parkinson, D. Y.; Yuan, R.; Hallinan, D. T.; MacDowell, A. A.; Balsara, N. P. Failure Mode of Lithium Metal Batteries with a Block Copolymer Electrolyte Analyzed by X-Ray Microtomography. *J. Electrochem. Soc.* **2015**, *162*, A1301–A1309.

(14) Chintapalli, M.; Le, T. N. P.; Venkatesan, N. R.; Mackay, N. G.; Rojas, A. A.; Thelen, J. L.; Chen, X. C.; Devaux, D.; Balsara, N. P. Structure and Ionic Conductivity of Polystyrene-*block*-poly(ethylene oxide) Electrolytes in the High Salt Concentration Limit. *Macromolecules* **2016**, *49*, 1770–1780.

(15) Lascaud, S.; Perrier, M.; Vallee, A.; Besner, S.; Prud'homme, J.; Armand, M. Phase Diagrams and Conductivity Behavior of Poly-(ethylene oxide)-Molten Salt Rubbery Electrolytes. *Macromolecules* **1994**, *27*, 7469–7477.

(16) Chintapalli, M.; Chen, X. C.; Thelen, J. L.; Teran, A. A.; Wang, X.; Garetz, B. A.; Balsara, N. P. Effect of Grain Size on the Ionic Conductivity of a Block Copolymer Electrolyte. *Macromolecules* **2014**, *47*, 5424–5431.

(17) Bruce, P. G.; Vincent, C. A. Steady state current flow in solid binary electrolyte cells. *J. Electroanal. Chem. Interfacial Electrochem.* **1987**, *225*, 1–17.

(18) Hayamizu, K.; Akiba, E.; Bando, T.; Aihara, Y. ^{1}H, ^{7}Li, and ^{19}F nuclear magnetic resonance and ionic conductivity studies for liquid electrolytes composed of glymes and polyetheneglycol dimethyl ethers of $CH_3O(CH_2CH_2O)_nCH_3$ (n = 3–50) doped with $LiN(SO_2CF_3)_2$. *J. Chem. Phys.* **2002**, *117*, 5929–5939.

(19) Chintapalli, M.; Timachova, K.; Olson, K. R.; Mecham, S. J.; Devaux, D.; DeSimone, J. M.; Balsara, N. P. Relationship between Conductivity, Ion Diffusion, and Transference Number in Perfluoropolyether Electrolytes. *Macromolecules* **2016**, *49*, 3508–3515.

(20) Timachova, K.; Watanabe, H.; Balsara, N. P. Effect of Molecular Weight and Salt Concentration on Ion Transport and the Transference Number in Polymer Electrolytes. *Macromolecules* **2015**, *48*, 7882–7888.

(21) Padhi, A. K.; Nanjundaswamy, K. S.; Goodenough, J. B. Phospho-olivines as Positive-Electrode Materials for Rechargeable Lithium Batteries. *J. Electrochem. Soc.* **1997**, *144*, 1188–1194.

(22) Zaghib, K.; Striebel, K.; Guerfi, A.; Shim, J.; Armand, M.; Gauthier, M. LiFePO$_4$/polymer/natural graphite: low cost Li-ion batteries. *Electrochim. Acta* **2004**, *50*, 263–270.

(23) Devaux, D.; Glé, D.; Phan, T. N. T.; Gigmes, D.; Giroud, E.; Deschamps, M.; Denoyel, R.; Bouchet, R. Optimization of Block Copolymer Electrolytes for Lithium Metal Batteries. *Chem. Mater.* **2015**, *27*, 4682–4692.

(24) Wang, J.; Liu, P.; Hicks-Garner, J.; Sherman, E.; Soukiazian, S.; Verbrugge, M.; Tataria, H.; Musser, J.; Finamore, P. Cycle-life model for graphite-LiFePO$_4$ cells. *J. Power Sources* **2011**, *196*, 3942–3948.

(25) Huang, Y.-H.; Goodenough, J. B. High-Rate LiFePO$_4$ Lithium Rechargeable Battery Promoted by Electrochemically Active Polymers. *Chem. Mater.* **2008**, *20*, 7237–7241.

(26) Porcarelli, L.; Shaplov, A. S.; Salsamendi, M.; Nair, J. R.; Vygodskii, Y. S.; Mecerreyes, D.; Gerbaldi, C. Single-Ion Block Copoly(ionic liquid)s as Electrolytes for All-Solid State Lithium Batteries. *ACS Appl. Mater. Interfaces* **2016**, *8*, 10350–10359.

(27) Srinivasan, V.; Newman, J. Discharge Model for the Lithium Iron-Phosphate Electrode. *J. Electrochem. Soc.* **2004**, *151*, A1517–A1529.